Canadian Science Publishing | Canadian Journal of Chemistry

High-dose-rate effects in the radiolysis of water at elevated temperatures.

Journal:	*Canadian Journal of Chemistry*
Manuscript ID	cjc-2021-0012.R1
Manuscript Type:	Article
Date Submitted by the Author:	04-Mar-2021
Complete List of Authors:	Sultana, Abida; Université de Sherbrooke, Nuclear Medicine and Radiobiology Meesungnoen, Jintana; D&#65533;partement de m&#65533;decine nucl&#65533;aire et de radiobiologie Jay-Gerin, Jean-Paul; Université de Sherbrooke, Médecine nucléaire et radiobiologie
Is the invited manuscript for consideration in a Special Issue? :	Not applicable (regular submission)
Keyword:	Liquid water, radiolysis, Absorbed dose rate, elevated temperatures, linear energy transfer (LET), Monte Carlo track chemistry simulations

High-dose-rate effects in the radiolysis of water at elevated temperatures

by

Abida Sultana,[(1)] Jintana Meesungnoen, and Jean-Paul Jay-Gerin[(*)]

Département de Médecine Nucléaire et de Radiobiologie, Faculté de Médecine et des Sciences de la Santé, Université de Sherbrooke, 3001, 12e Avenue Nord, Sherbrooke (Québec) J1H 5N4, Canada. *E-mail:* jean-paul.jay-gerin@USherbrooke.ca

[(1)] On leave from the Department of Applied Chemistry and Chemical Engineering, Noakhali Science and Technology University, Noakhali, 3814, Bangladesh.

[(*)] Corresponding author.

Canadian Journal of Chemistry
Manuscript ID: cjc-2021-0012.R1
March 16, 2021

Abstract:

Monte Carlo track chemistry simulations were used to study the effects of high dose rates on the radical (e^-_{aq}, $H^\bullet$, and $^\bullet OH$) and molecular (H_2 and H_2O_2) yields in the low linear energy transfer (LET) radiolysis of liquid water at elevated temperatures between 25–350 °C. Our simulation model consisted of randomly irradiating water with single pulses of *N* incident protons of 300 MeV (LET ~ 0.3 keV/μm), which penetrate at the same time perpendicular to this water within the surface of a circle. The effect of dose rate was studied by varying *N*. Our simulations showed that, at any given temperature, the radical products decrease with increasing dose rate and, at the same time, the molecular products increase, resulting from an increase in the inter-track, radical-radical reactions. Using the kinetics of the decay of hydrated electrons at 25 and 350 °C, we determined a critical time (τ_c), for each value of *N*, which corresponds to the "onset" of dose-rate effects. For our irradiation model, τ_c was inversely proportional to *N* for the two temperatures considered, with τ_c at 350 °C shifted by an order of magnitude to shorter times compared to its values at 25 °C. Finally, the data obtained from the simulations for *N* = 2,000 generally agreed with the observation that during the track stage of radiolysis, free radical yields increase, while molecular products decrease with increasing temperatures from 25 to 350 °C. The exceptions of e^-_{aq} and H_2 to this general pattern are briefly discussed.

Keywords: Liquid water, radiolysis, absorbed dose rate, linear energy transfer (LET), elevated temperatures, Monte Carlo track chemistry simulations.

1. Introduction

The "primary" products that are generated by radiolysis of liquid water (or dilute aqueous solutions)[1,2] include the hydrated electron (e^-_{aq}), $H^\bullet$, H_2, $^\bullet OH$, H_2O_2, H_3O^+, OH^-, *etc*. Of these, the radicals e^-_{aq} and $^\bullet OH$ are produced in the highest concentrations. Under normal irradiation conditions, it is assumed that the *dose rate* (energy absorbed by the system per unit of mass per unit of time) is sufficiently low that the distance between individual tracks is so great that they can be regarded as isolated. In such a situation, the history of only one track needs to be considered and the radiolysis yields (or *G* values) are independent of the dose rate and characteristic of the quality of the radiation (a descriptor is the "linear energy transfer" or LET).[3] However, as the dose rate increases, so does the number of isolated tracks that are present at the same time, which reduces the average distance between neighboring tracks. *The onset of dose-rate effects occurs when this distance becomes sufficiently small that an interaction (overlap) occurs between adjacent tracks*.[4]

In the case of low-LET radiation, the various radiolytic products are initially formed in high local concentration in small, widely separated Magee-type "spurs"[5] along the track of the incident radiation, due to the physics of energy deposition. At low dose rates, these spurs develop independently of one another over time until they merge and homogeneity is established in the bulk of the solution (on the μs timescale at 25 °C).[6] In this case, the predominant effect of radiolysis is the formation of free radicals (e^-_{aq}, $H^\bullet$, and $^\bullet OH$). At high dose rates, this situation changes due to the spatial proximity of the radiation tracks, which leads to increased yields of inter-track radical-radical reactions, which occur even before the intra-track spur reactions are completed. Under these conditions, the proportion of molecular products (H_2, H_2O_2 and reformed water) increases at the expense of the radical products. This

dependence of the radiolytic yields on the dose rate agrees very well with existing experimental data and modeling studies.[7-26]

In recent work,[26] we studied the effects of very high dose rates on the transient yields of radical and molecular species formed during radiolysis of water by 300-MeV incident protons, which mimic the low-LET of ^{60}Co γ rays or a beam of energetic (*e.g.*, MeV) electrons. In fact, all of these radiations have the same LET of ~0.3 keV/μm at 25 °C.[27,28] In the current study, in order to gain further insight into the effects of the dose rate on the variation in primary chemical yields, we performed Monte Carlo simulations of the radiolysis of neat, deaerated liquid water under conditions of high dose rates as a function of temperature up to 350 °C. This work is of importance in the nuclear power industry, where radiolysis products cause corrosion of in-core materials (by changing the "water chemistry") and activity transport (transport of radioactive material from the reactor core).[29-32] It is particularly relevant for water-cooled nuclear reactors under severe – accidental or emergency – conditions where radiation dose rates can vary over a very wide range up to ~10^{10} Gy/s or more.[33]

2. Simulation model

A) Modeling dose-rate effects

We used a simulation model[26] that consists of the random irradiation of water with single and instantaneous pulses of N incident 300-MeV protons (LET ~ 0.3 keV/μm), which penetrate this water perpendicularly over the surface of a circle with the radius R_o (see Fig. 1). This is the so-called "model of the instantaneous pulse", in which the pulse duration is assumed to be zero.[34] The advantage of using energetic protons is that their trajectories are rectilinear, which makes it possible to define a *cylindrical geometry* of the beam at the time of entry. In this geometry, the proton tracks are all-parallel to the cylinder's axis. This two-dimensional (2D) geometric model is clearly

advantageous in the problem at hand compared to fast-electron beam irradiation, in which (spherical) spurs are randomly distributed in 3D over the entire irradiated volume. The proton tracks that were initially contained in this cylinder, are obviously not restricted to this volume, but develop throughout the bulk water (infinitely in fact) as a function of time via the diffusion of the various radiolytic species that were initially formed in it. This problem is very similar to the one we have dealt with for many years in Monte Carlo simulations of the radiolysis of water,[6] with the exception that here, instead of simulating a single proton track at a time (limit of low dose rate) (*e.g.*, ref. 3), we simulate N interactive tracks simultaneously.

Under these conditions, the effect of the dose rate is studied by simply varying N, or yet the "fluence" defined as $N/\pi R_o^2$, where πR_o^2 is the area of the circular base of the cylinder.

B) Monte Carlo track-chemistry simulations

Our Monte Carlo track-chemistry computer code IONLYS-IRT[6] was used to simulate the radiolysis of deaerated liquid water by 300-MeV irradiating protons. A detailed description of this code at both ambient and high temperatures has been reported elsewhere.[3,6,35-40] Only a brief overview of its most essential features is given below.

Our code first models the early *physical and physicochemical stages* of the radiation action up to ~1 ps in track development in a 3D geometric environment ("IONLYS" program). Since our program can only simulate the spatio-temporal course of one proton track at a time, we have modified it so that simultaneously incident proton tracks in close spatial proximity can be calculated.[26] In this study, the number of impacting protons per pulse[41] was chosen to vary from N = 1 (one single-proton irradiation that mimics ^{60}Co γ-ray or fast electron irradiation) to 2,000. These N

protons reach the front of the cylinder at the same time (chosen as time zero) and travel parallel to the positive *Y*-axis (Fig. 1).

The complex spatial distribution of the reactants of the considered track system at the end of the physicochemical stage is provided as an output of the IONLYS program. It is then used directly as the starting point for the subsequent *chemical stage*. This stage in which the different radiolytic species randomly diffuse at rates determined by their diffusion coefficients and react with each other (or in competition with dissolved solutes present in the solution at the time of irradiation), is covered by our "IRT" program (>1 ps). This program uses the "independent reaction times" or IRT method,[36,42,43] a computationally efficient stochastic simulation technique that simulates reaction times without having to follow the trajectories of the diffusing species. Its implementation has been described elsewhere.[36] The ability of this method to give accurate time-dependent chemical yields over a wide range of irradiation conditions has been well validated by comparison with full random flights (or step-by-step) Monte Carlo simulations,[44,45] which follow the trajectories of the reactants in detail. While the consideration of a large number of proton trajectories for the implementation of our IRT program at high dose rates was not a particular problem, the obviously longer computation times than for the simulation of single trajectories were the only disadvantage.

The reaction scheme, rate constants, and diffusion coefficients used in our IRT program for pure, deaerated water in the 25–350 °C temperature range are the same as those previously used.[40,46,47] All Monte Carlo simulations were performed along the liquid-vapor coexistence curve, with the density of pressurized water decreasing from ~1 g/cm^3 at 25 °C to ~0.892 g/cm^3 (~0.893 MPa) at 175 °C, and to ~0.575 g/cm^3 (~16.5 MPa) at 350 °C.[48] In this temperature range, calculations show that *G* values of transient species depend relatively little on the pressure (or density) applied.

All calculations were performed by simulating short (~100 μm) segments of 300-MeV incident proton tracks (see Fig. 1). The energy and the LET of the protons were well defined over these simulated track segments and remained nearly constant. For a given value of *N*, the number of simulation "histories" (typically 3–100, depending on *N*) was chosen to ensure only minor statistical fluctuations (less than 1–3 %) in the computed averages of chemical yields,[49] while keeping acceptable computer time limits.

3. Results and discussion

(A) *Radiolysis of pure deaerated water at high dose rates, at 25 and 350 °C*

Figure 2A–J shows the temporal variation of the radical (e^-_{aq}, •OH, and H•) and molecular (H_2 and H_2O_2) yields as a function of *N*, as obtained from our simulations of the radiolysis of pure, air-free liquid water by 300-MeV irradiating protons at 25 and 350 °C, in the interval ~1 ps–10 μs. For clarity, we only show the curves for *N* = 1, 100, 500, 1,000, and 2,000 here. Data for *N* = 1, indicating the limit of low dose rates (*i.e.*, with no overlap between the tracks of different incident protons),[3,40] mimic radiolysis of water with ^{60}Co γ rays or fast electrons and are used as a reference. Using our previous calibration of *N* in terms of dose rates (expressed in Gy/s) at 25 °C (see Fig. 3B of ref. 26),[41] the above values of *N* correspond to dose rates of ~3×10^8 (*N* = 100), 1.9×10^9 (*N* = 500), 4.2×10^9 (*N* = 1,000), and 8.7×10^9 (*N* = 2,000) Gy/s under our irradiation conditions.

As shown in Fig. 2, for each species at both 25 and 350 °C, the yields at ~1 ps are nearly the same irrespective of *N*. With increasing time, the different yields initially remain unchanged regardless of *N*, until a critical time (τ_c) is reached, after which the different yield curves begin to deviate from their respective one-single proton irradiation (*N* = 1) reference curves. As can be seen, at a given temperature, with

increasing *N*, these deviations occur at ever shorter times and with a greater amplitude. This critical time, which clearly depends on *N* and decreases with increasing temperature from 25 to 350 °C, can be viewed as a *signature of the "onset" of dose-rate effects in the solution*.[26] We will determine τ_c as a function of *N* and temperature in the next section based on the results of the hydrated electron yields.

As a general rule, *at 25 °C, the radical yields decrease with increasing N while at the same time the molecular yields increase*. This is due to the increasing importance of inter-track, radical-radical combination/recombination reactions in the irradiated solutions, which in turn leads to the formation of more molecular products. This trend in our calculated yield values agrees well with previously published experimental and theoretical work.[7-25] This has already been described in detail in ref. 26 and is therefore not discussed further here.

At 350 °C, the same rule also applies but one point worth mentioning in Fig. 2 is the rather peculiar time profiles of $G(^{\bullet}OH)$ and $G(H_2)$, as well as of $G(H^{\bullet})$, above ~0.1 μs in the homogeneous chemical stage of the radiolysis. Indeed, under conditions without dose-rate effects (*N* = 1), $G(^{\bullet}OH)$ and $G(H_2)$ show quite a large increase (Fig. 2D and H) while $G(H^{\bullet})$ decreases accordingly (Fig. 2F). The mechanism directly responsible for these behaviors is the oxidation of water by $H^{\bullet}$ atoms:[40,46]

(1) $H^{\bullet} + H_2O \rightarrow H_2 + {}^{\bullet}OH$,

which is negligibly slow at ambient temperature but accelerates quickly at elevated temperatures with a rate constant $k_1 = (5.9 \pm 1.5) \times 10^4\ M^{-1}\ s^{-1}$ at 350 °C.[51] As can be seen from Fig. 2, when dose-rate effects develop, the contribution of reaction (1) to the production of $^{\bullet}OH$ and H_2 decreases rapidly. The reason for this result is that with increasing *N* the probability of inter-track reactions in the bulk of the solution increases, which leads to growing competition between radical-radical reactions and

reaction (1). This means that an increasing number of H• atoms in the nonhomogeneous stage of the radiolysis are involved in inter-radical reactions *before* they even have the opportunity to react with water.

(B) ***The "onset" of dose-rate effects at 25 and 350 °C***

As seen above, τ_c is interpreted as the minimum time before interaction between tracks occurs.[4,26] To determine τ_c we used the same method as that developed in ref. 26. In short, this method consists of subtracting the $G(e^-_{aq})$ versus time values that correspond to the simulation of N interacting proton tracks from those obtained for single-proton irradiation. It should be noted that the kinetics of the decay of hydrated electrons were used here simply because e^-_{aq} is the first radiolytic species to interact with a neighboring track. This is due firstly to the large penetration range of the low-energy ("dry") secondary electrons (prior to hydration)[52,53] and secondly to the high diffusion coefficient of e^-_{aq}.[40]

Figure 3 compares the variation of our calculated values of τ_c as a function of N in a log-log plot at 25 and 350 °C. As the figure shows, there is a similar linear relationship between the logarithms of τ_c and N for the two temperatures, with the two corresponding straight lines being practically parallel over the entire range of values of N considered here. Moreover, Fig. 3 shows that under the same irradiation conditions, the straight line obtained at 350 °C is simply shifted by about a decade (one order of magnitude) to shorter times compared to that at 25 °C. For instance, for N = 2,000, τ_c varies from ~120 ps at 25 °C to ~13 ps at 350 °C. Qualitatively, this result was expected as reflecting the effect of high temperatures on the radiolytic process and the accelerated development of radiation tracks.[37-40,47] The present calculations therefore make it possible *to quantify* this difference.

The linearity of the logarithms of τ_c and N (*i.e.*, the dose rate) observed in Fig. 3 indicates that the variation of τ_c with N can be represented as:

$$\tau_c = \frac{C}{(N)^n}, \quad (2)$$

where C is a constant of proportionality and the 99% confidence interval of the exponent actually contains the value $n = 1$.[26] In other words, for our cylindrical irradiation model, the "onset" of dose-rate effects for the two temperatures studied is inversely proportional to N. If we further assume that there is a linear relationship between N and the dose rate (in Gy/s) not only at 25 °C[41] but at any temperature including 350 °C,[54] then we can conclude that just like at 25 °C, τ_c also varies inversely with the dose rate at 350 °C.

(C) *High-dose-rate radiolysis of pure deaerated water as a function of temperature between 25 and 350 °C*

Figure 4A–J shows the time profiles of $G(e^-_{aq})$, $G(^{\bullet}OH)$, $G(H^{\bullet})$, $G(H_2)$, and $G(H_2O_2)$ as obtained from our Monte Carlo simulations of the radiolysis of pure, air-free liquid water by N = 2,000 300-MeV incident protons at various temperatures between 25–350 °C for the interval of ~1 ps–10 μs. For comparison purposes, data obtained from the simulation for $N = 1$,[40] which corresponds to the limit of low dose rates, are used here. To the best of our knowledge, these high-temperature chemical yield calculations are the first to be performed for such high-dose-rate irradiations. Unfortunately, under these irradiation conditions, no experimental data are available to compare with our results.

As discussed above, for each species, the yields initially remain nearly unchanged until the critical time τ_c is reached, after which the different curves begin to deviate from the respective $N = 1$ reference curves. Our simulations show that *at any given*

temperature the radical products e^-_{aq} and $^\bullet OH$ decrease[55] *with increasing dose rate, while at the same time the molecular products H_2 and H_2O_2 increase*. This reflects the increasing intervention of radical-radical reactions,[26] which allows fewer radicals to escape combination and recombination reactions during the expansion of the tracks, which in turn leads to higher molecular yields. With increasing temperature from 25 to 350 °C, the data obtained from the simulation for N = 2,000 are generally consistent with the observation[46,56] that during the track stage of the radiolysis, the yields of free radicals increase continuously, while we have lower yields of molecular products (with the exception of e^-_{aq} and H_2; see below). This is explained[37,57-59] by the fact that many combination/recombination reactions are not diffusion-controlled and therefore have rate constants that increase less with temperature than the diffusion of the individual species. The faster diffusion of these species at high temperatures increases their likelihood of escaping track reactions, thus resulting in higher radical yields.

Figure 4A shows that for N = 2,000 $G(e^-_{aq})$ decreases with increasing temperature. This is contrary to what one would have expected. To better understand the origin of this decrease, one can simply examine the unfolding of the various reactions involved. This is done in Fig. 5A and B, where we compare, at 25 and 350 °C, the cumulative yield variations, $\Delta G(e^-_{aq})$, for each of the reactions that contribute to the yield of e^-_{aq}. As we can see, the observed decrease in $G(e^-_{aq})$ is mainly due to the reaction of e^-_{aq} with hydronium ions and with $^\bullet OH$ radicals, according to:[47,60]

(3) $e^-_{aq} + H_3O^+ \rightarrow H^\bullet + H_2O \quad k_3 = 2.13 \times 10^{10}\ M^{-1}\ s^{-1}$ (25 °C)
$= 2.07 \times 10^{12}\ M^{-1}\ s^{-1}$ (350 °C)

(4) $e^-_{aq} + {}^\bullet OH \rightarrow OH^- \quad k_4 = 3.55 \times 10^{10}\ M^{-1}\ s^{-1}$ (25 °C)
$= 4.77 \times 10^{11}\ M^{-1}\ s^{-1}$ (350 °C),

where k_3 and k_4 are the rate constants of the two individual reactions. There are also relatively small contributions due to the reactions of e^-_{aq} with itself, $H^\bullet$, and H_2O_2. Note that the rate constant for the self-reaction of the hydrated electron: $e^-_{aq} + e^-_{aq}$ (+ $2H_2O$) $\rightarrow H_2 + 2OH^-$ drops abruptly above ~150 °C.[47,56,61] As a result, more and more hydrated electrons become available as the temperature increases to either react in other intra- or inter-track reactions such as reactions (3) and (4) or to escape into the bulk of the solution. Compared to the results at 25 °C, where $G(e^-_{aq})$ decreases mainly due to the reaction of e^-_{aq} with $^\bullet OH$, Fig. 5A and B shows that the order of importance of reactions (3) and (4) is completely reversed at 350 °C: the contribution of the H_3O^+ reaction with e^-_{aq} is greater at 350 °C (approximately 2 *G*-units at ~10 ns) than at 25 °C and becomes largely predominant. This is understandable, since the rate constant for this reaction increases with temperature much more steeply than that for reaction (4). These results therefore explain the faster decay kinetics of $G(e^-_{aq})$ which are observed at 350 °C.

Although H_2 is a molecular product, it is observed that $G(H_2)$ increases with temperature. The cause of this anomalous increase in H_2 formation for the low-LET, low-dose-rate (*i.e.*, $N = 1$) radiolysis of pure, deaerated liquid water between 25–350 °C has been examined in detail elsewhere.[62,63] As with $N = 1$, the increase in $G(H_2)$ with temperature for $N = 2{,}000$ is largely due to low-energy, electron-driven processes that occur at very short times (<1 ps) rather than to intra- or inter-track radical-radical reactions involving e^-_{aq} and $H^\bullet$ atoms. This is clearly indicated in Fig. 5C and D, where we show the time profiles of the extents $\Delta G(H_2)$ of the various components of $G(H_2)$ calculated from our Monte Carlo simulations from 1 ps to 10 μs. Recall here that these early time processes include the "dissociative electron attachment" (or DEA), the recombination of subexcitation electrons with their geminate cations $H_2O^{\bullet+}$, and the dissociation of directly excited water molecules (for a review, see ref. 62). Figure 5C

and D shows that these three processes contribute to H_2 formation at 1 ps, ~0.25 molecule/100 eV at 25 °C. This contribution increases to ~0.46 molecule/100 eV at 350 °C. Since they occur in the sub-picosecond time scale,[62] however, *the effects of the dose rate do not influence these processes*.

Finally, as noted above, the oxidation of water by $H^{\bullet}$ atoms in the homogeneous chemical stage at 350 °C offers another process for H_2 formation (~0.62 molecule/100 eV; see Fig. 5D), which is not present at 25 °C. Interestingly, this contribution is much smaller for N = 2,000 than for N = 1 (Fig. 4G and H). This is due to the increasing number of $H^{\bullet}$ atoms in the track chemistry of the radiolysis which are involved in inter-radical reactions *before* they have a chance to react with water for N = 2,000.

4. Conclusion

Monte Carlo track chemistry simulations were used in an attempt to quantify the effects of high dose rates on the yields of the primary radical and molecular species formed in the radiolysis of pure, deaerated liquid water at elevated temperatures from 25 to 350 °C. In the current work, we simulated the irradiation of water by 300-MeV incident protons, which mimic the low-LET limit of ^{60}Co γ rays or energetic electrons.

The results obtained for a cylindrical, “instantaneous pulse” irradiation model, showed that at any temperature the molecular yields increase with increasing dose rate. Simultaneously, the radical yields decrease, a direct consequence of the increased probability of inter-track radical-radical combination or recombination reactions throughout the solution.

Using the kinetics of the decay of hydrated electrons at 25 and 350 °C, we were able to determine the “critical time” τ_c at which the interaction between tracks starts to occur. For both temperatures, this “onset” of dose-rate effects was inversely

proportional to *N*, the "number of irradiating protons per pulse" (*i.e.*, the dose rate). Interestingly, the values of τ_c at 350 °C were simply shifted by an order of magnitude to shorter times compared to its corresponding values at 25 °C, which clearly reflects the effect of high temperatures on the radiolytic process and the accelerated development of radiation tracks.

Moreover, the data obtained from the simulation of the radiolysis of deaerated water by *N* = 2,000 proton tracks per pulse followed the general pattern of increasing the free radical yields and simultaneously reducing the molecular yields with increasing temperature from 25 to 350 °C.

To the best of our knowledge, these high-temperature chemical yield calculations are the first to be performed in such a high dose rate range where experimental data are not yet available. Nevertheless, experimental data are essential to describe the dependence of the radiolytic yields under these irradiation conditions and of course to validate our modeling approach.

Acknowledgements

We thank Professor Yusa Muroya (Osaka University, Japan) for valuable comments and very stimulating correspondence. The research of J.-P.J-G. is supported by the NSERC Discovery Grant No. RGPIN-2015-06100.

References

(1) Spinks, J. W. T.; Woods, R. J. *An introduction to radiation chemistry*, 3rd ed. Wiley, New York, 1990.

(2) Ferradini, C.; Jay-Gerin, J.-P. *Can. J. Chem.* **1999**, *77*, 1542.

(3) Alanazi, A.; Meesungnoen, J.; Jay-Gerin, J.-P. *Can. J. Chem.* **2020**, *98*, 427.

(4) Kuppermann, A. In: M. Haïssinsky, Editor. *Actions chimiques et biologiques des radiations.* Masson, Paris, 1961; vol. 5, pp. 85–166.

(5) Magee, J. L. *Annu. Rev. Nucl. Sci.* **1953**, *3*, 171.

(6) Meesungnoen, J.; Jay-Gerin, J.-P. In: Y. Hatano, Y. Katsumura, and A. Mozumder, Editors. *Charged particles and photon interactions with matter. Recent advances, applications, and interfaces.* Taylor & Francis, Boca Raton, FL, 2011; pp. 355–400.

(7) Keene, J. P. *Radiat. Res.* **1957**, *6*, 424.

(8) Sutton, H. C.; Roblat, J. *Nature* **1957**, *180*, 1332.

(9) Roblat, J.; Sutton, H. C. *Proc. Roy. Soc. (London) Ser. A* **1960**, *255*, 490.

(10) Anderson, A. R.; Hart, E. J. *J. Phys. Chem.* **1962**, *66*, 70.

(11) Thomas, J. K.; Hart, E. J. *Radiat. Res.* **1962**, *17*, 408.

(12) Burns, W. G.; Barker, R. In: G. Porter, Editor. *Progress in reaction kinetics*. Pergamon, Oxford, 1965; vol. 3, p. 303–368.

(13) Willis, C.; Boyd, A. W.; Rothwell, A. E.; Miller, O. A. *Int. J. Radiat. Phys. Chem.* **1969**, *1*, 373.

(14) Sehested, K.; Bjergbakke, E.; Holm, N. W.; Fricke, H. *Dosimetry in agriculture, industry, biology and medicine.* International Atomic Energy Agency (IAEA) Publication STI/PUB/311. IAEA, Vienna, Austria, 1973; pp. 397–404.

(15) Muller, J.-C.; Ferradini, C.; Pucheault, J. *Int. J. Radiat. Phys. Chem.* **1975**, *7*, 635.

(16) Pucheault, J.; Ferradini, C.; Gardès, M.; Lesigne, B.; Gilles, L.; Muller, J.-C. *Int. J. Chem. Kinet.* **1977**, *9*, 603.

(17) Fanning, J. E., Jr.; Trumbore, C. N.; Barkley, P. G.; Short, D. R.; Olson, J. H. *J. Phys. Chem.* **1977**, *81*, 1026.

(18) Fanning, J. E., Jr.; Trumbore, C. N.; Barkley, P. G.; Olson, J. H. *J. Phys. Chem.* **1977**, *81*, 1264.

(19) Trumbore, C. N.; Short, D. R.; Fanning, J. E., Jr.; Olson, J. H. *J. Phys. Chem.* **1978**, *82*, 2762.

(20) Shiraishi, H.; Katsumura, Y.; Hiroishi, D.; Ishigure, K.; Washio, M. *J. Phys. Chem.* **1988**, *92*, 3011.

(21) Trupin-Wasselin, V. Ph.D. thesis, Université Paris XI, Orsay, France, 2000 (https://bit.ly/362hBPP).

(22) Watanabe, R.; Saito, K. *Radiat. Phys. Chem.* **2001**, *62*, 217.

(23) Kreipl, M. S.; Friedland, W.; Paretzke, H. G. *Radiat. Environ. Biophys.* **2009**, *48*, 349.

(24) Schneider, N. M.; Norton, M. M.; Mendel, B. J.; Grogan, J. M., Ross, F. M.; Bau, H. H. *J. Phys. Chem. C* **2014**, *118*, 22373.

(25) Ramos-Méndez, J.; Domínguez-Kondo, N.; Schuemann, J.; McNamara, A.; Moreno-Barbosa, E.; Faddegon, B. *Radiat. Res.* **2020**, *194*, 351.

(26) Alanazi, A.; Meesungnoen, J.; Jay-Gerin, J.-P. *Radiat. Res.* **2021**, *195*, 149.

(27) Watt, D. E. *Quantities for dosimetry of ionizing radiations in liquid water*. Taylor & Francis, London, UK, 1996.

(28) Note that the similarity between the track structures of a 300-MeV proton and a Compton electron ejected from the absorption of a cobalt-60 γ ray in liquid water has already been described in detail elsewhere (*e.g.*, Mustaree, S.; Meesungnoen, J.; Butarbutar, S. L.; Causey, P.; Stuart, C. R.; Jay-Gerin, J.-P. *RSC Adv.* **2014**, *4*, 43572).

(29) Boyd, A. W., Editor. *Determination of absorbed dose in reactors*. Technical Report STI/DOC/10/127. International Atomic Energy Agency (IAEA), Vienna, Austria, 1971.

(30) McCracken, D. R.; Tsang, K. T.; Laughton, P. J. *Aspects of the physics and chemistry of water radiolysis by fast neutrons and fast electrons in nuclear reactors*. Report AECL-11895. Atomic Energy of Canada Limited, Chalk River, Ont., 1998.

(31) Kritsky, V. G. *Water chemistry and corrosion of nuclear power plant structural materials*. American Nuclear Society, La Grange Park, IL, 1999.

(32) Guzonas, D.; Novotny, R.; Penttilä, S.; Toivonen, A.; Zheng, W. *Materials and water chemistry for supercritical water-cooled reactors*. Woodhead Publishing (Elsevier), Duxford, UK, 2018.

(33) Muroya, Y., 2021, personal communication. Note that typical absorbed dose rates in the current generation of water-cooled nuclear reactors during normal operation are of the order of 10^3 kGy/h, *i.e.*, about 300 Gy/s (refs. 29–32).

(34) *The dosimetry of pulsed radiation*. ICRU Report No. 34. International Commission on Radiation Units and Measurements, Bethesda, MD, 1982.

(35) Cobut, V.; Frongillo, Y.; Patau, J. P.; Goulet, T.; Fraser, M.-J.; Jay-Gerin, J.-P. Radiat. Phys. Chem. **1998**, *51*, 229.

(36) Frongillo, Y.; Goulet, T.; Fraser, M.-J.; Cobut, V.; Patau, J. P.; Jay-Gerin, J.-P. *Radiat. Phys. Chem.* **1998**, *51*, 245.

(37) Hervé du Penhoat, M.-A.; Goulet, T.; Frongillo, Y.; Fraser, M.-J.; Bernat, P.; Jay-Gerin, J.-P. *J. Phys. Chem. A* **2000**, *104*, 11757.

(38) Tippayamontri, T.; Sunuchakan, S.; Meesungnoen, J.; Sunaryo, G. R.; Jay-Gerin, J.-P. In: S. G. Pandalai, Editor. *Recent research developments in physical chemistry*. Transworld Research Network, Trivandrum, Kerala, India, 2009; vol. 10, pp. 143–211.

(39) Patwary, Md M.; Kanike, V.; Sanguanmith, S.; Meesungnoen, J.; Islam, M. M.; Jay-Gerin, J.-P. *Phys. Chem. Chem. Phys.* **2019**, *21*, 7137.

(40) Sultana, A.; Meesungnoen, J.; Jay-Gerin, J.-P. *Phys. Chem. Chem. Phys.* **2020**, *22*, 7430.

(41) In ref. 26, we used experimental data (from refs. 14 and 21) of the yield $G(Fe^{3+})$ of the "super-Fricke" dosimeter (oxygen-saturated solution of 10 mM $FeSO_4$ in aqueous 0.4 M H_2SO_4) as a function of dose rate up to ~10^{10} Gy/s to *calibrate* N, the "number of incident protons per pulse", in terms of "dose rate" (in Gy/s) at room temperature. The resulting calibration curve was well described by a

straight line over most of the range of values of *N* considered here. Under our irradiation conditions, *N* = 2,000 is equivalent to an absorbed dose rate of ~8.7 × 10^9 Gy/s at 25 °C.

(42) Tachiya, M. *Radiat. Phys. Chem.* **1983**, *21*, 167.

(43) Pimblott, S. M.; Pilling, M. J.; Green, N. J. B. *Radiat. Phys. Chem.* **1991**, *37*, 377.

(44) Goulet, T.; Fraser, M.-J.; Frongillo, Y.; Jay-Gerin, J.-P. *Radiat. Phys. Chem.* **1998**, *51*, 85.

(45) Plante, I. Ph.D. thesis, Université de Sherbrooke, Sherbrooke, Que., 2009.

(46) Sanguanmith, S.; Meesungnoen, J.; Jay-Gerin, J.-P. *Chem. Phys. Lett.* **2013**, *588*, 82.

(47) Elliot, A. J.; Bartels, D. M. *The reaction set, rate constants and g-values for the simulation of the radiolysis of light water over the range 20° to 350 °C based on information available in 2008*. Report AECL No. 153-127160-450-001. Atomic Energy of Canada Ltd., Chalk River, Ont., 2009.

(48) Lemmon, E. W.; Huber, M. L.; McLinden, M. O. NIST Standard Reference Database 23: *Reference fluid thermodynamic and transport properties – REFPROP*, Version 9.0. National Institute of Standards and Technology, U.S. Department of Commerce, Gaithersburg, MD, 2010.

(49) It is worth noting that radiation chemical yields are traditionally described in terms of *G* values, *G*(X) being the total number of the species X formed or consumed per 100 eV of energy absorbed. Throughout this article, *G* values are quoted in units of "molecule per 100 eV". For conversion into SI units (mol J^{-1}): 1 molecule per 100 eV ≈ 0.10364 μmol J^{-1} (refs. 1 and 2).

(50) Sanguanmith, S.; Meesungnoen, J.; Muroya, Y.; Lin, M.; Katsumura, Y.; Jay-Gerin, J.-P. *Phys. Chem. Chem. Phys.* **2012**, *14*, 16731.

(51) Muroya, Y.; Yamashita, S.; Lertnaisat, P.; Sanguanmith, S.; Meesungnoen, J.; Jay-Gerin, J.-P.; Katsumura, Y. *Phys. Chem. Chem. Phys.* **2017**, *19*, 30834.

(52) Meesungnoen, J.; Jay-Gerin, J.-P.; Filali-Mouhim, A.; Mankhetkorn, S. *Radiat. Res.* **2002**, *158*, 657.

(53) Muroya, Y.; Sanguanmith, S.; Meesungnoen, J.; Lin, M.; Yan, Y.; Katsumura, Y.; Jay-Gerin, J.-P. *Phys. Chem. Chem. Phys.* **2012**, *14*, 14325.

(54) Unfortunately, due to the lack of experimental data on the radiolysis of liquid water at high temperatures under high dose-rate irradiation conditions, we could not use the same method here at 350 °C as that developed in ref. 26 at 25 °C to calibrate *N* as a function of the dose rate (in Gy/s).

(55) Contrary to the behavior of the other radical yields, $G(H^{\bullet})$ increases with increasing dose rate. This rather peculiar time profile of $G(H^{\bullet})$ has been discussed in detail in ref. 26.

(56) Sanguanmith, S.; Muroya, Y.; Meesungnoen, J.; Lin, M.; Katsumura, Y.; Mirsaleh Kohan, L.; Guzonas, D.; Stuart, C. R.; Jay-Gerin, J.-P. *Chem. Phys. Lett.* **2011**, *508*, 224.

(57) Elliot, A. J.; Chenier, D. C.; Ouellette, D. C. *J. Chem. Soc., Faraday Trans.* **1993**, *89*, 1193.

(58) Elliot, A. J. *Rate constants and g-values for the simulation of the radiolysis of light water over the range 0–300 °C*. Report AECL-11073. Atomic Energy of Canada Ltd., Chalk River, Ont., 1994.

(59) Swiatla-Wojcik, D.; Buxton, G. V. *J. Phys. Chem.* **1995**, *99*, 11464.

(60) Kanike, V.; Meesungnoen, J.; Sanguanmith, S.; Guzonas, D.; Stuart, C. R.; Jay-Gerin, J.-P. *CNL Nucl. Rev.* **2017**, *6*, 31.

(61) Sanguanmith, S.; Meesungnoen, J.; Guzonas, D.; Stuart, C. R.; Jay-Gerin, J.-P. *J. Nucl. Eng. Radiat. Sci.* **2016**, *2*, 021014.

(62) Meesungnoen, J.; Sanguanmith, S.; Jay-Gerin, J.-P. *RSC Adv.* **2015**, *5*, 76813.

(63) Sterniczuk, M.; Bartels, D. M. *J. Phys. Chem. A* **2016**, *120*, 200.

Figure captions

Figure 1:

Illustration of the simulation model used in this work with a pulse of fifteen 300-MeV incident protons (LET ~ 0.3 keV/μm), which (randomly and simultaneously) impact perpendicularly on the water surface (*XZ* plane) within a circle of radius R_o = 0.1 μm. The figure shows a 3D representation of the proton tracks traversing through the water calculated from our IONLYS Monte Carlo code. All protons travel along the *Y*-axis over the entire track length chosen for the calculations (~100 μm). Energetic secondary electrons (δ rays), which define the so-called "penumbra", can also be seen surrounding the central track "cores". Obviously, since this irradiated cylindrical volume is embedded in non-irradiated bulk water, the radiolytic species initially formed there are not restricted to this volume, but rather diffuse throughout the entire bulk water as a function of time.

Figure 2:

Comparison of the effect of the dose rate (described here by *N*, the "number of irradiating protons per pulse") on the temporal variation of the radical and molecular yields (given in molecules per 100 eV) of the radiolysis of pure, deaerated water by 300-MeV incident protons obtained from our Monte Carlo simulations at 25 and 350 °C, over the interval of ~1 ps to 10 μs. Panels A–J show our e^-_{aq}, •OH, H•, H_2 and H_2O_2 yield results for *N* = 100 (dash line), 500 (dash-dot line), 1,000 (dash-dot-dot line) and 2,000 (dot line). Data for *N* = 1 (solid line) correspond to the limit of low dose rates (*i.e.*, with no interaction between tracks) and mimic the radiolysis of water by ^{60}Co γ rays or fast electrons; they are used here as a reference. The thin vertical lines shown at ~0.2 μs (at 25 °C) and at ~35 ns (at 350 °C) in the different panels indicate

the end of track expansion in the absence of dose-rate effects (ref. 50), *i.e.*, the time required to change from nonhomogeneous track kinetics to homogeneous kinetics in the bulk water.

Figure 3:

Log-log plot showing the variation in the critical time (τ_c, in second) for the "onset" of dose-rate effects, *i.e.*, the time at which inter-track reactions start to occur in the radiolysis of pure, deaerated liquid water by 300-MeV protons at 25 and 350 °C, as a function of *N*, the number of incident protons per pulse (*N* varying from 5 to 2,000), for the cylindrical irradiation model of Fig. 1. The method used to determine τ_c at both temperatures is explained in the text (see also ref. 26). The straight lines were obtained from a least-squares fit of the log(τ_c) *vs.* log(*N*) data at the two temperatures considered.

Figure 4:

Panels A–J show the effect of the dose rate on the temporal development of the radical (e^-_{aq}, $^{\bullet}OH$, and $H^{\bullet}$) and molecular (H_2 and H_2O_2) yields (in molecules per 100 eV), for *N* (the "number of incident protons per pulse") = 2,000 and *N* = 1 from our Monte Carlo simulations of the radiolysis of pure, deaerated water by 300-MeV irradiating protons at different temperatures: 25 (dot line), 100 (dash-dot-dot line), 200 (dash-dot line), 300 (dash line), and 350 (solid line) °C, over the interval of ~1 ps to 10 μs. Data for *N* = 1 indicating the limit of low dose rates (*i.e.*, without interaction between tracks) (ref. 40), mimic the radiolysis of water with ^{60}Co γ rays or fast electrons and are used here as a reference.

Figure 5:

Time dependence of the extents $\Delta G(e^-_{aq})$ and $\Delta G(H_2)$ (in molecule per 100 eV) of the main reactions that contribute to the yield of the hydrated electron and of molecular hydrogen on the ps–10 μs time scale (see text), calculated from our Monte Carlo simulations of the radiolysis of pure, deaerated liquid water by 300-MeV irradiating protons for *N* (the "number of incident protons per pulse") = 2,000, at 25 °C (Panels A and C) and 350 °C (Panels B and D).

FIGURE 1

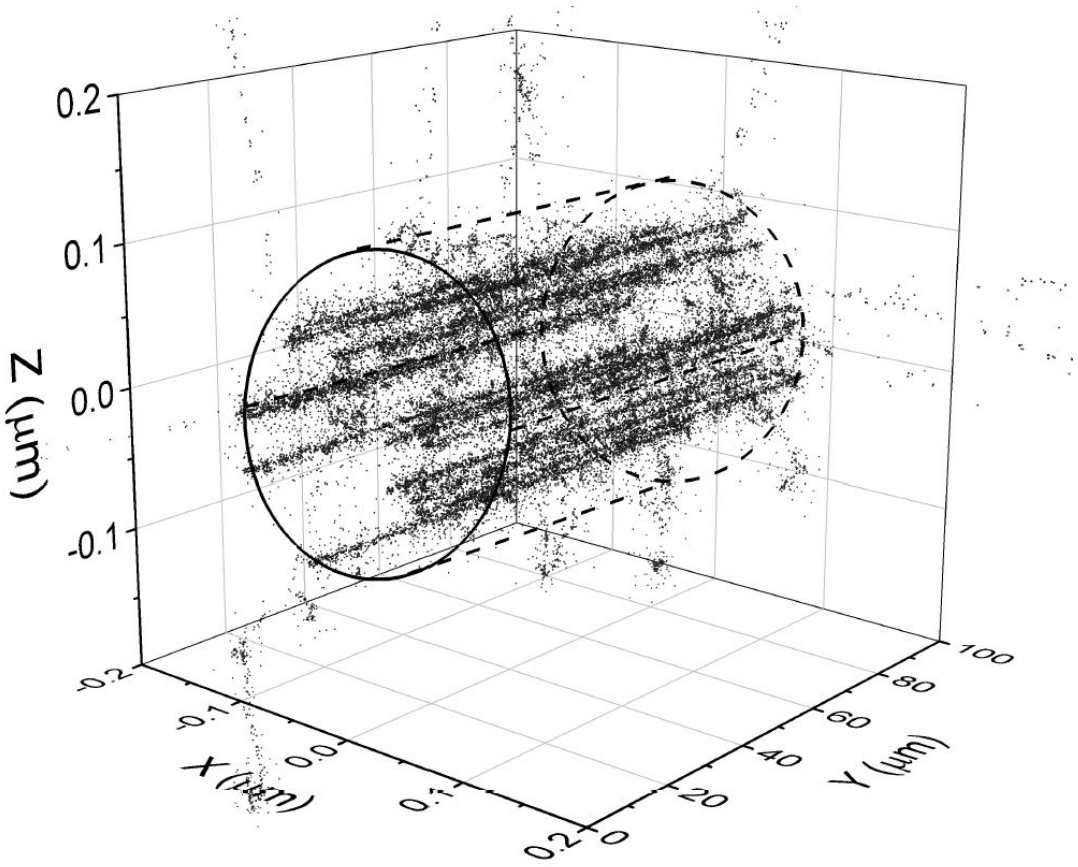

FIGURE 2

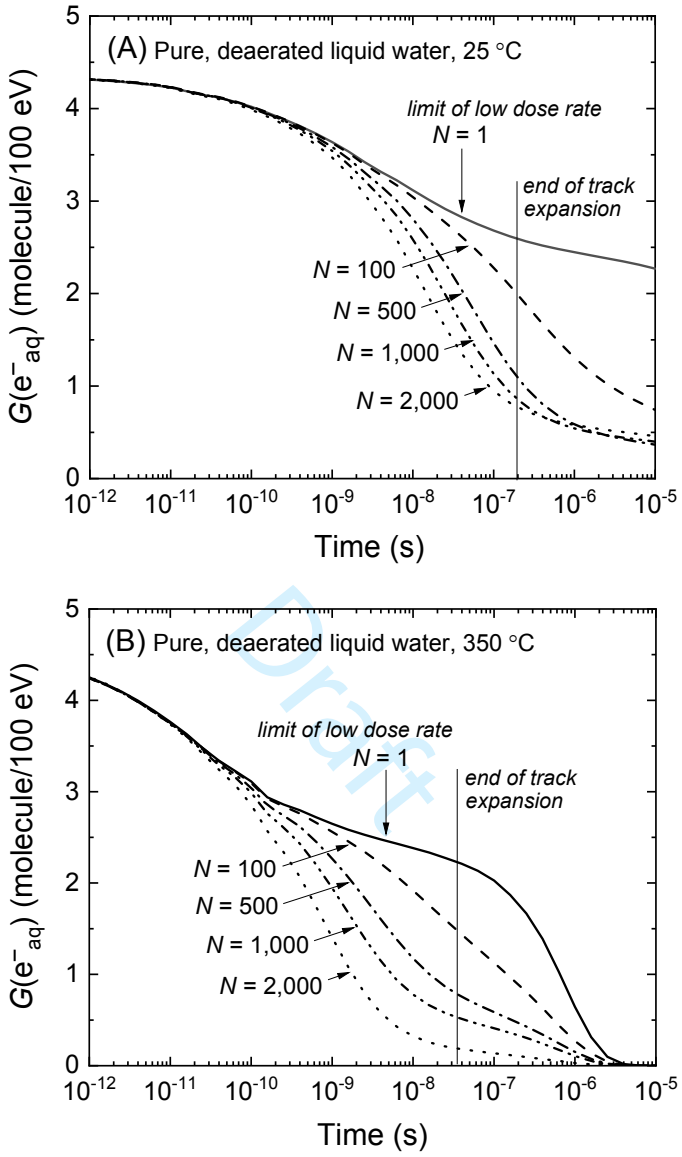

FIGURE 2 (Continued)

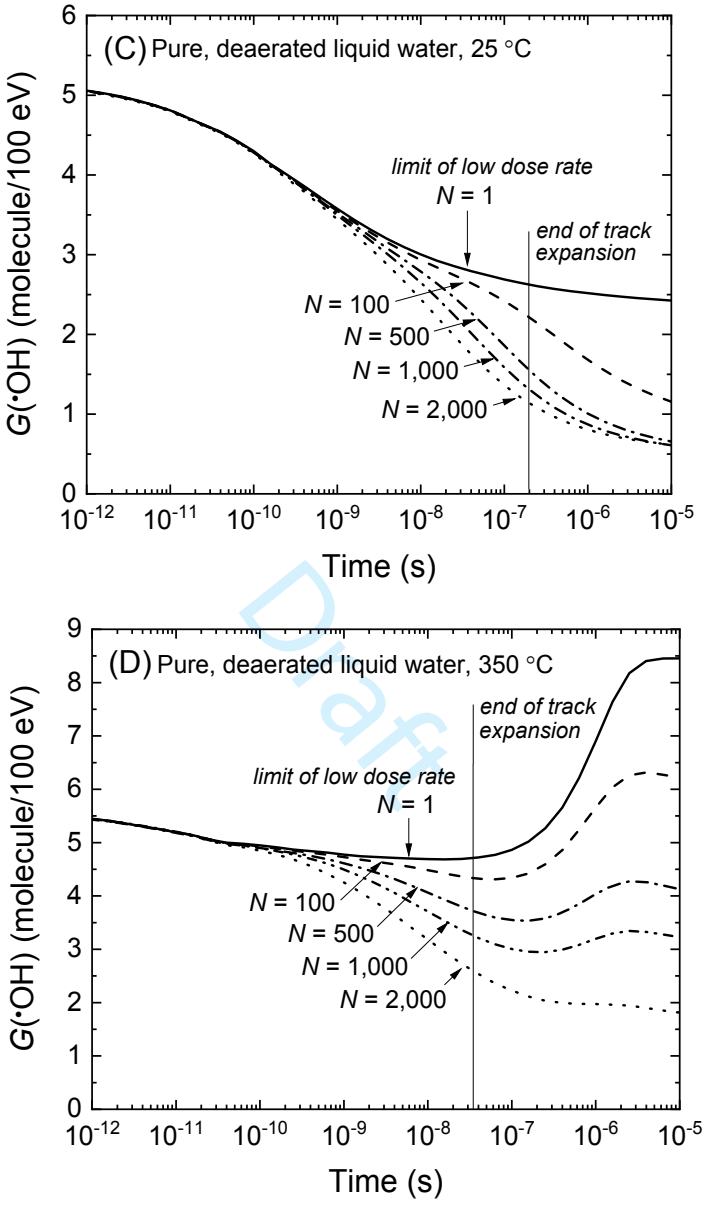

FIGURE 2 (Continued)

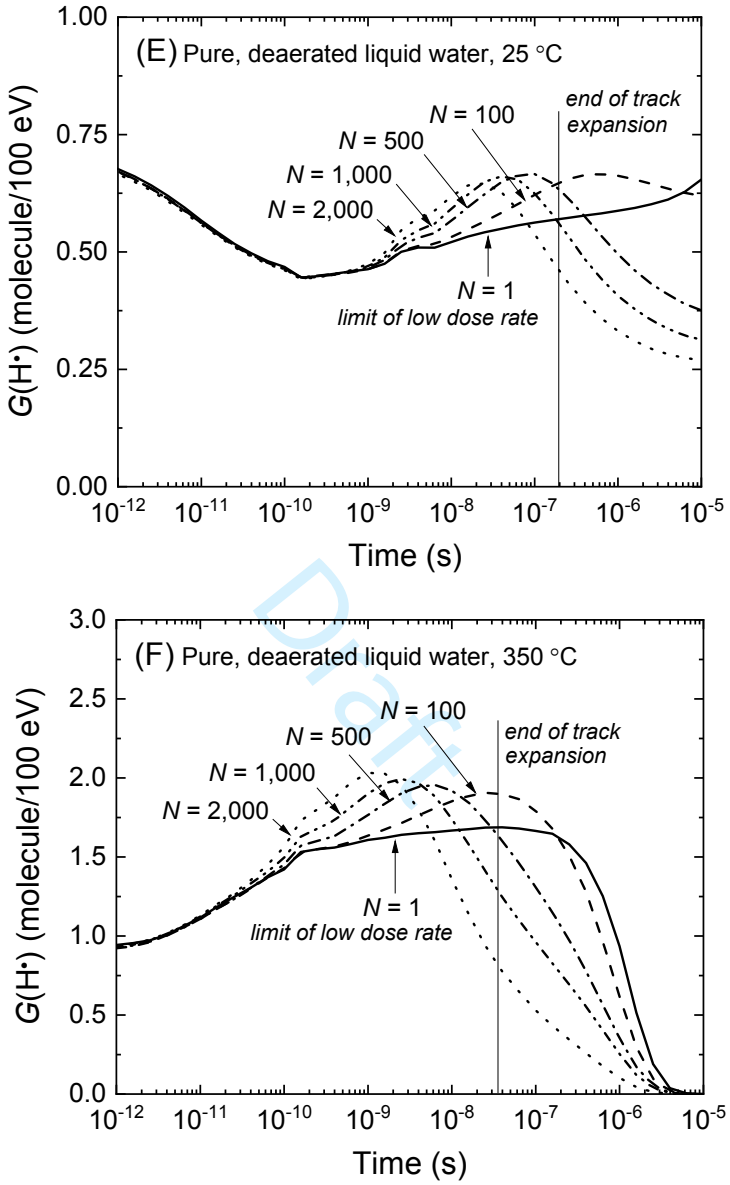

FIGURE 2 (Continued)

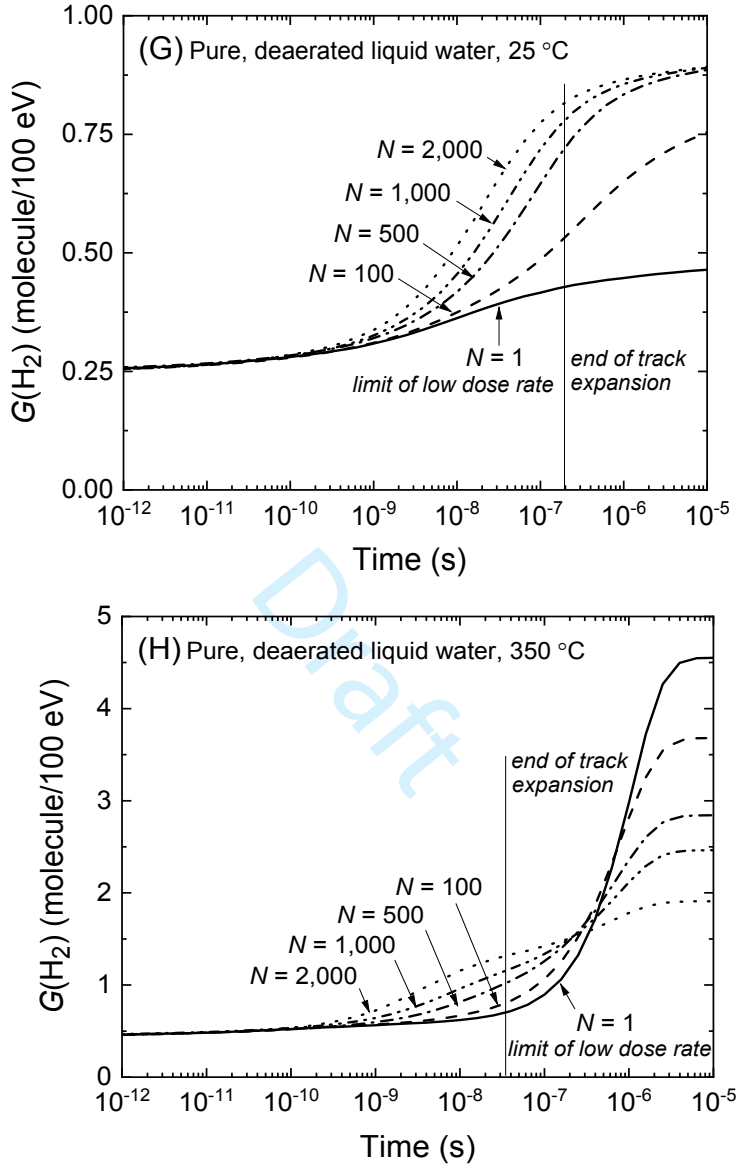

FIGURE 2 (Continued)

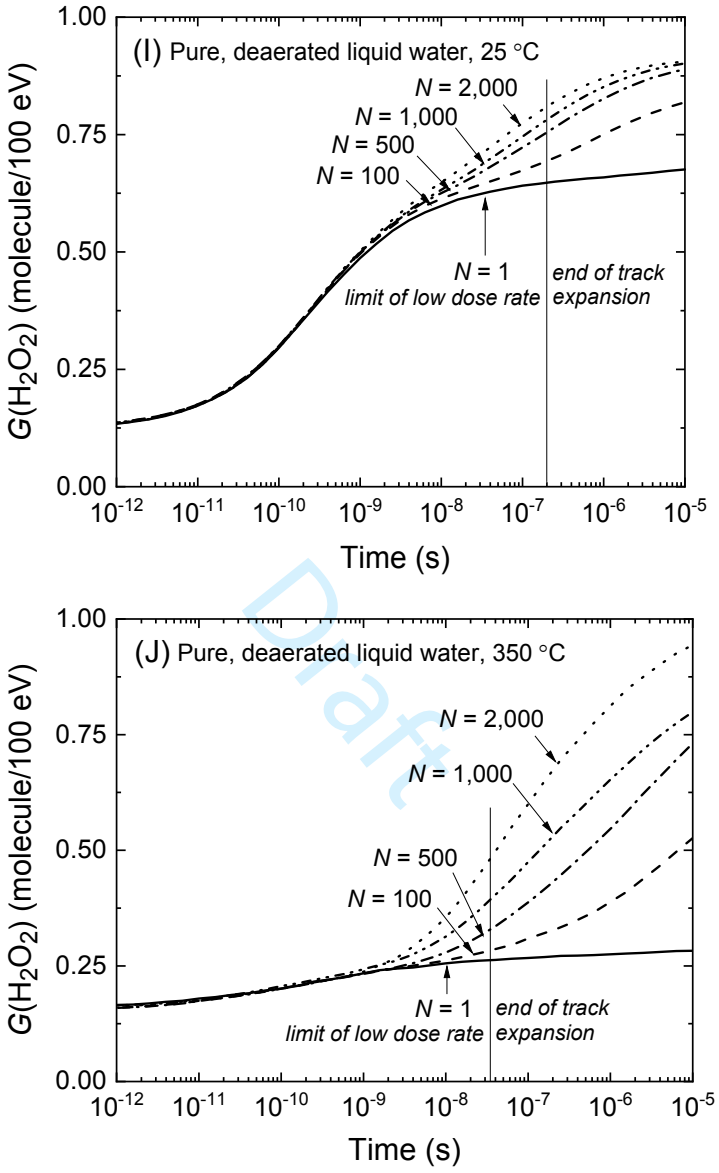

FIGURE 3

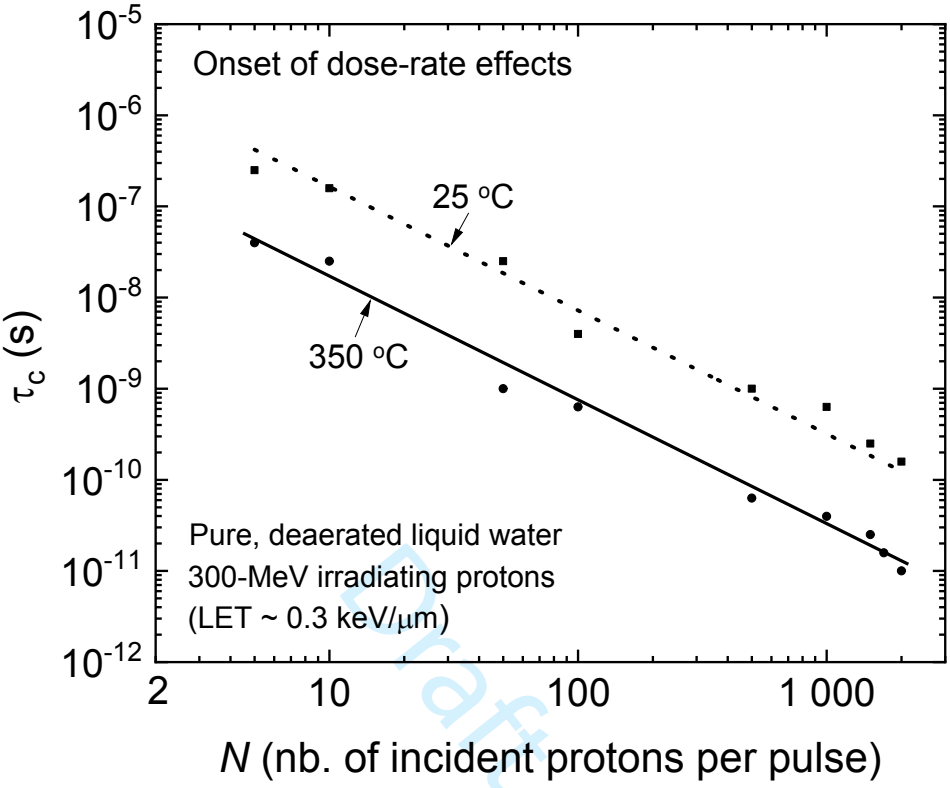

FIGURE 4

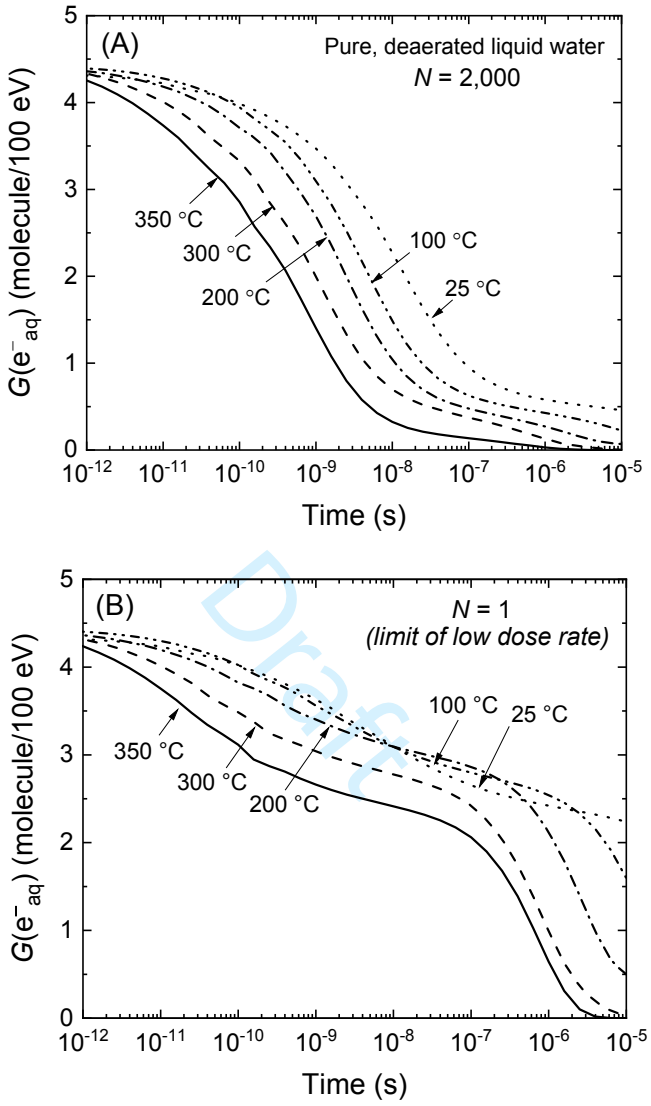

FIGURE 4 (Continued)

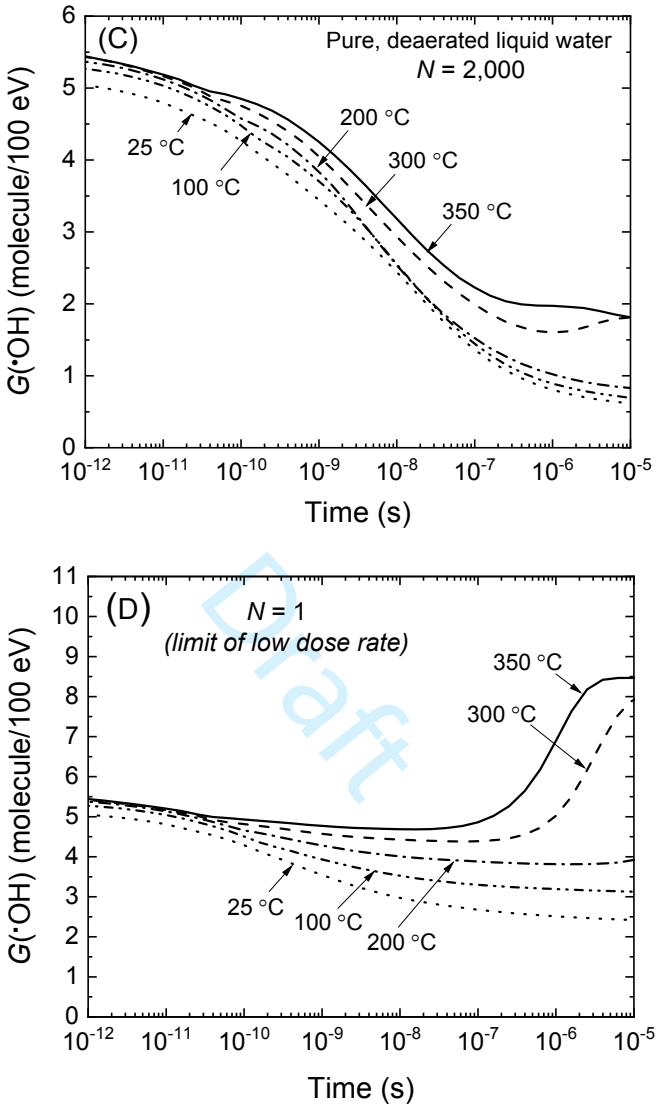

FIGURE 4 (Continued)

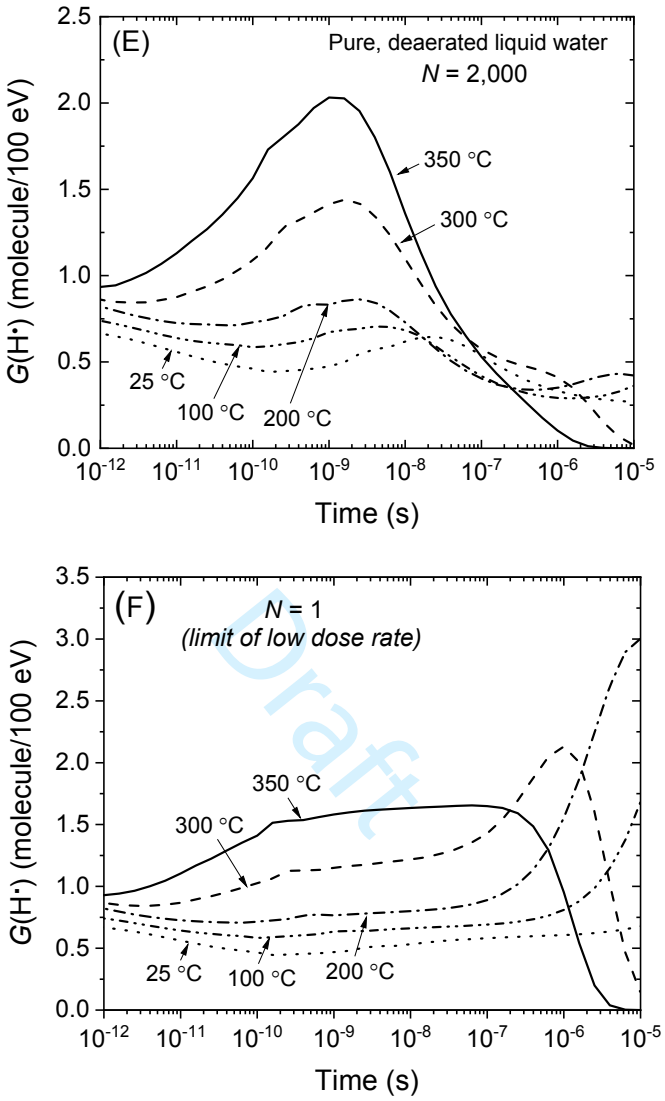

FIGURE 4 (Continued)

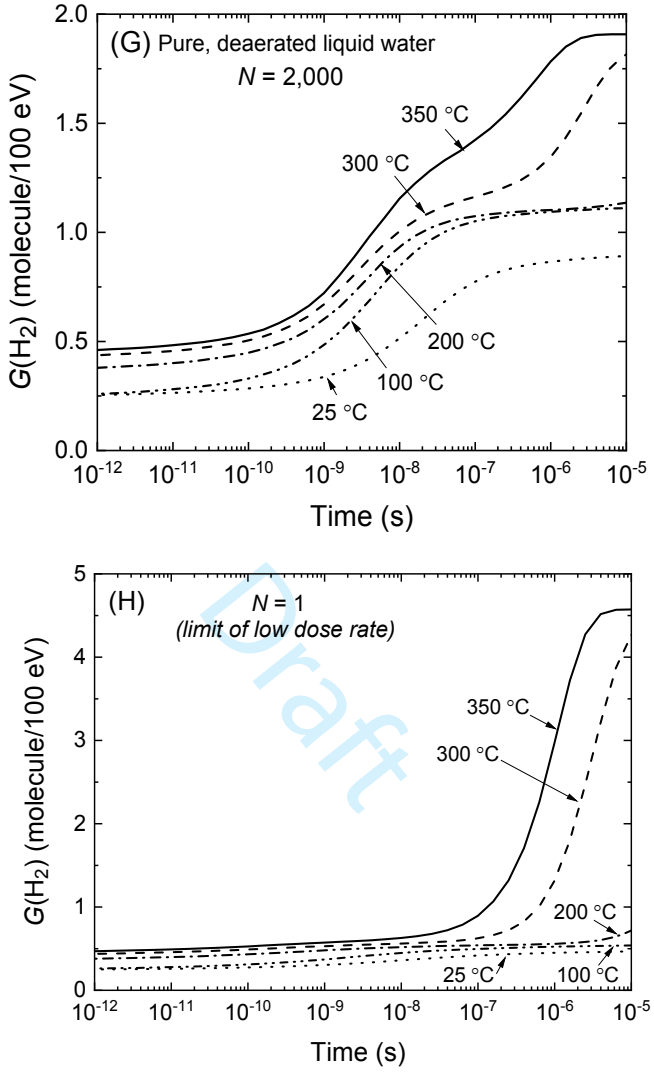

FIGURE 4 (Continued)

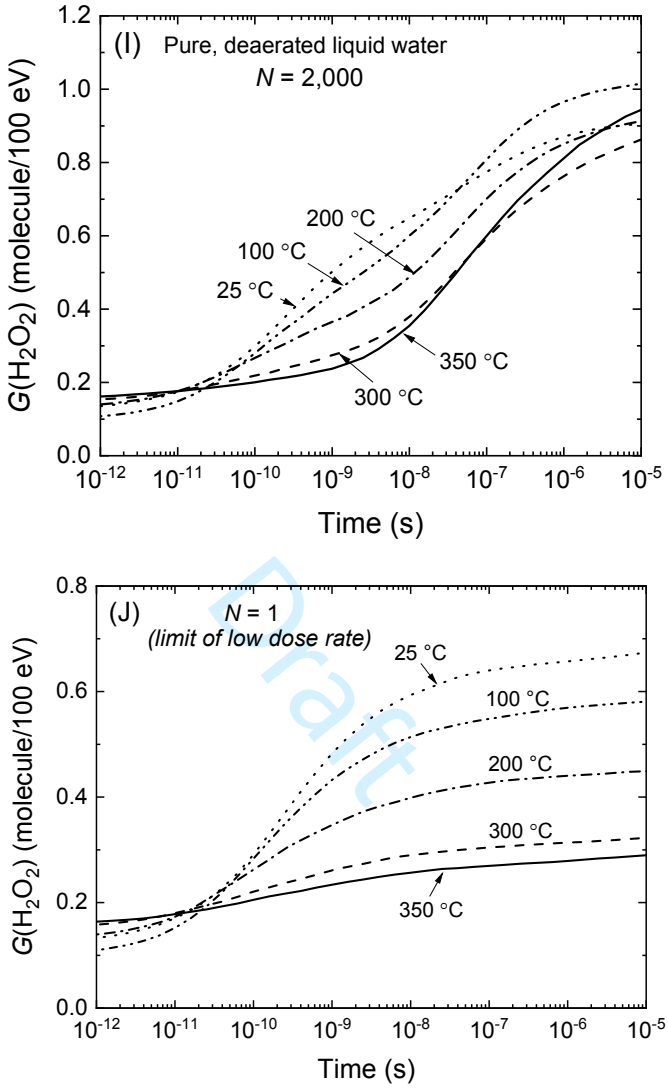

FIGURE 5

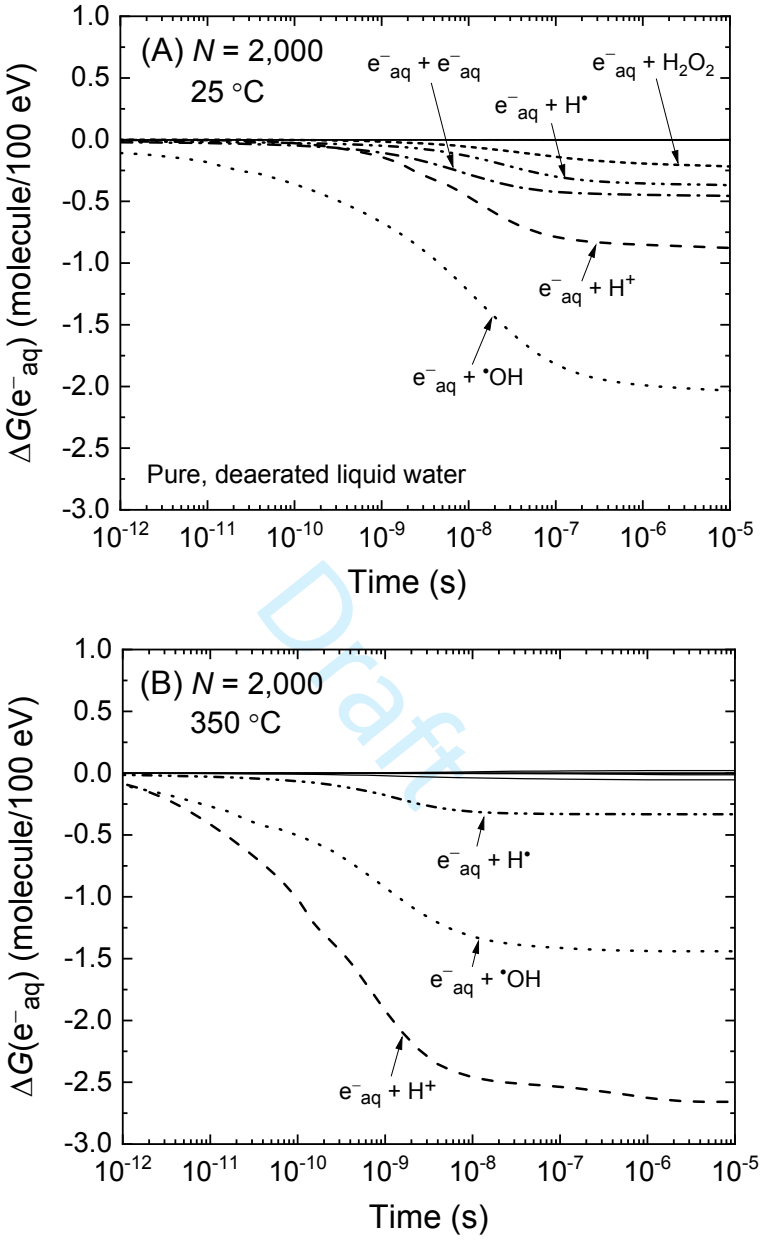

FIGURE 5 (Continued)